

Asymptotic self-similar blow up profile for 3-D Euler via physics-informed neural networks

Yongji Wang^{*}, Ching-Yao Lai[†], Javier Gómez-Serrano[‡], Tristan Buckmaster[§]

Abstract

We develop a new numerical framework, employing physics-informed neural networks, to find a smooth self-similar solution for the Boussinesq equations. The solution corresponds to an asymptotic self-similar profile for the 3-dimensional Euler equations in the presence of a cylindrical boundary. In particular, the solution represents a precise description of the Luo-Hou blow-up scenario [G. Luo, T. Hou, Proc. Natl. Acad. Sci. 111(36): 12968–12973, 2014] for the 3-dimensional Euler equations. To the best of the authors' knowledge, the solution is the first truly multi-dimensional smooth backwards self-similar profile found for an equation from fluid mechanics. The new numerical framework is shown to be both robust and readily adaptable to other equations.

Significance

This paper sheds light on the question of finite time blow-up for the 2-dimensional Boussinesq and the 3-dimensional Euler equations with boundary, questions of fundamental importance to the field of mathematical fluid mechanics. Using a novel numerical method employing physics-informed neural networks, we construct a smooth backwards self-similar solution for the Boussinesq equations. The solution itself could potentially form the basis of a future computer-assisted proof of blow-up for the 2-dimensional Boussinesq and the 3-dimensional Euler equations with boundary.

1 Introduction

1.1 The Boussinesq equations

The Boussinesq equation is an equation on two spatial dimensions that can be written as

$$\partial_t \mathbf{u} + \mathbf{u} \cdot \nabla \mathbf{u} + \nabla p = (0, \theta), \quad \operatorname{div} \mathbf{u} = 0 \quad \text{and} \quad \partial_t \theta + \mathbf{u} \cdot \nabla \theta = 0, \quad (1.1)$$

where the 2D vector $\mathbf{u}(\mathbf{x}, t)$ is the velocity and the scalar $\theta(\mathbf{x}, t)$ is the temperature. The spatial variable \mathbf{x} is taken on the half plane $x_2 \geq 0$ and we impose the non-penetration boundary condition $u_2(x_1, 0) = 0$.

The question of singularity formation from smooth initial data for the Boussinesq equation is one of the fundamental questions in fluid mechanics, mentioned in Yudovich's '*Eleven great problems of mathematical hydrodynamics*' [30]. As pointed out by Luo and Hou [22], the problem is intrinsically linked to the problem of singularity formation for the 3-D Euler in the presence of a cylindrical boundary (cf. [3, 9, 11, 23]). Indeed, the mechanism for blow-up for Boussinesq is believed to be identical to that of 3-D Euler with cylindrical boundary, as will be elaborated on in Section 2.1.

^{*}Department of Geosciences, Princeton University Princeton, NJ yw1705@princeton.edu

[†]Department of Geosciences, Princeton University Princeton, NJ cylai@princeton.edu

[‡]Department of Mathematics, Brown University, Providence RI & Departament de Matemàtiques i Informàtica, Universitat de Barcelona, Barcelona javier.gomez-serrano@brown.edu / jgomez-serrano@ub.edu

[§](Corresponding Author) Department of Mathematics, Princeton University, Princeton, NJ & School of Mathematics, Institute for Advanced Study Princeton, NJ buckmaster@math.princeton.edu / tbuckmaster@ias.edu

Self-similar blow-up is known to occur from non-smooth $C^{1,\alpha}$, $\alpha > 0$ small initial data. This was shown in [3], building off the groundbreaking work of Elgindi, who proved a similar result for 3-D Euler [8] (cf. [12]). The question of finite-time blow-up from smooth initial data however remains unresolved.

We also mention the numerical work [17] of Guillod and Šverák where they find smooth forward self-similar solutions for the axi-symmetric 3-D Navier-Stokes equation.

In the search for singularity formation for the Boussinesq equations, we look for *backwards* self-similar solutions to (1.1) of the form

$$\mathbf{u} = (1-t)^\lambda \mathbf{U}(\mathbf{y}), \quad \theta = (1-t)^{-1+\lambda} \Theta(\mathbf{y}), \quad (1.2)$$

where we define the self-similar coordinates as

$$\mathbf{y} = (y_1, y_2) = \frac{(x_1, x_2)}{(1-t)^{1+\lambda}}. \quad (1.3)$$

Under the ansatz (1.2), the equations (1.1) become

$$\begin{aligned} -\lambda \mathbf{U} + ((1+\lambda)\mathbf{y} + \mathbf{U}) \cdot \nabla \mathbf{U} + \nabla P &= (0, \Theta) \\ (1-\lambda)\Theta + ((1+\lambda)\mathbf{y} + \mathbf{U}) \cdot \nabla \Theta &= 0 \\ \operatorname{div} \mathbf{U} &= 0 \end{aligned} \quad (1.4)$$

for an implicitly defined $P : \mathbb{R}^2 \rightarrow \mathbb{R}$. The corresponding solution will be expected to have infinite energy; however, we will impose that the solution to (1.4) will have mild growth at infinity which should allow such a solution to be *cut-off* to produce an asymptotically self-similar solution with a finite-time singularity (cf. [12]).

1.2 Physics-informed neural networks (PINNs)

Physics-informed neural networks (PINNs) were developed in 2019 by Raissi et al. [27, 28]. PINNs are a new class of numerical solver for partial differential equations (PDE) and have been widely used in science and engineering [19]. In this work, we leverage the power of PINNs in solution searching with imposed constraints to find self-similar solutions to PDEs. To the best of our knowledge, this is the first use of a PINN to construct self-similar solutions. PINNs leverage the fact that neural networks are universal function approximators [18] and can theoretically approximate desired functions to arbitrary precision, including solutions to PDEs. In PINNs, neural networks approximate the solution to a PDE by searching for a solution in a continuous domain that approximately satisfies the physics constraints (e.g. initial conditions, boundary conditions and the equation itself). Instead of calculating the solution at the next time step using the solution at the current time step and a discretized PDE, a PINN calculates the imposed constraints in a continuous domain using the PINN solution, and updates the PINN solution until the neural network's optimization algorithm finds a solution that closely satisfies the imposed constraints. By imposing the self-similar equations (1.2), the boundary conditions, and symmetry assumptions as PINN constraints, we train a PINN to find the self-similar solution (\mathbf{U}, Θ) defined in (1.4).

PINNs have been successfully used to solve not only forward problems but also inverse problems (e.g. identifying Reynolds number from a given flow and the Navier-Stokes equation [27]), demonstrating the capacity of PINNs to invert for unknown parameters in the imposed constraints. Here we use a PINN to find not only the self similar solution profile but also the unknown self-similarity exponent λ defined in (1.2).

2 Smooth self-similar blow-up profile for Boussinesq equations

It is helpful to rewrite (1.4) in vorticity form. If we set $\Omega = \operatorname{curl} \mathbf{U} = \partial_{y_1} U_2 - \partial_{y_2} U_1$, $\Phi = \partial_{y_1} \Theta$ and $\Psi = \partial_{y_2} \Theta$, we obtain the equations

$$\begin{aligned} \Omega + ((1+\lambda)\mathbf{y} + \mathbf{U}) \cdot \nabla \Omega &= \Phi \\ (2 + \partial_{y_1} U_1)\Phi + ((1+\lambda)\mathbf{y} + \mathbf{U}) \cdot \nabla \Phi &= -\partial_{y_1} U_2 \Psi \\ (2 + \partial_{y_2} U_2)\Psi + ((1+\lambda)\mathbf{y} + \mathbf{U}) \cdot \nabla \Psi &= -\partial_{y_2} U_1 \Phi \\ \operatorname{div} \mathbf{U} &= 0 \end{aligned} \quad (2.1)$$

In order to reduce the complexity of finding solutions to (2.1), we will impose the following symmetry assumptions: U_1 is odd and (U_2, Θ) are even in the y_1 direction. Consequently, we have (Φ, Ω) are odd; whereas, Ψ is even in the y_1 direction. We will in addition impose

$$U_2(y_1, 0) = 0, \quad \text{and} \quad \Theta(0, y_2) = 0. \quad (2.2)$$

The first condition is a consequence of the non-penetration boundary condition. In order to remove a symmetry, we add the constraint

$$\partial_{y_1} \Omega(0) = -1.$$

Finally, in order to rule out extraneous solutions, we impose that $\nabla \mathbf{U}$, Φ and Ψ all vanish at infinity.

2.1 Luo-Hou scenario for Euler blow-up in the presence of boundary

The 3-D Euler equations, under axi-symmetry take the form

$$\begin{aligned} (\partial_t + u_r \partial_r + u_3 \partial_{x_3}) \left(\frac{\omega_\theta}{r} \right) &= \frac{1}{r^4} \partial_{x_3} (ru_\theta)^2 \\ (\partial_t + u_r \partial_r + u_3 \partial_{x_3}) (ru_\theta) &= 0 \\ \omega_\theta &= \partial_{x_3} u_r - \partial_r u_3 \end{aligned}$$

where here (u_r, u_θ, u_3) is the velocity in cylindrical coordinates and ω_θ is the angular component of the vorticity. We will introduce a cylindrical boundary at $r = 1$, and restrict ourselves to the exterior domain $\{(r, x_3) \in r \geq 1, x_3 \in \mathbb{R}\}$.

Luo and Hou in [22] (cf. [23]) performed compelling numerical simulations proposing a new scenario for finite time blow-up of the axi-symmetric 3-D Euler equations in the presence of a cylindrical boundary.¹ Luo and Hou simulated the time dependent problem and observed a dramatic growth (by a factor of $3 \cdot 10^8$) in the L^∞ norm of the vorticity, strongly suggesting a finite time singularity. Their simulations also suggest that the singularity is asymptotically self-similar.

Motivated by the work of Luo and Hou, we make the self-similar ansatz

$$\begin{aligned} (u_r, u_{x_3}) &= (1-t)^\lambda \mathbf{U}(\mathbf{y}, s) = (1-t)^\lambda (U_1(\mathbf{y}, s), U_2(\mathbf{y}, s)), \\ \omega_\theta &= (1-t)^{-1} \Omega(\mathbf{y}, s), \quad \partial_r (ru_\theta)^2 = (1-t)^{-2} \Psi(\mathbf{y}, s), \quad \partial_{x_3} (ru_\theta)^2 = (1-t)^{-2} \Phi(\mathbf{y}, s) \end{aligned}$$

where we define our self-similar coordinates as

$$\mathbf{y} = (y_1, y_2) = \frac{(x_3, r-1)}{(1-t)^{1+\lambda}}, \quad s = -\log(1-t).$$

Under the above ansatz, we obtain the equations

$$\begin{aligned} (\partial_s + 1) \Omega + ((1+\lambda)\mathbf{y} + \mathbf{U}) \cdot \nabla \Omega &= \Phi + \mathcal{E}_1 \\ (\partial_s + 2 + \partial_{y_1} U_1) \Phi + ((1+\lambda)\mathbf{y} + \mathbf{U}) \cdot \nabla \Phi &= -\partial_{y_1} U_2 \Psi \\ (\partial_s + 2 + \partial_{y_2} U_2) \Psi + ((1+\lambda)\mathbf{y} + \mathbf{U}) \cdot \nabla \Psi &= -\partial_{y_2} U_1 \Phi \\ \operatorname{div} \mathbf{U} &= \mathcal{E}_2 \end{aligned} \quad (2.3)$$

where the errors \mathcal{E}_1 and \mathcal{E}_2 are given by the expressions

$$\begin{aligned} \mathcal{E}_1 &= -y_2 e^{-(1+\lambda)s} \frac{(y_2 e^{-(1+\lambda)s} + 2)(y_2^2 e^{-2(1+\lambda)s} + 2y_2 e^{-(1+\lambda)s} + 2)}{(1 + y_2 e^{-(1+\lambda)s})^4} \Phi \\ \mathcal{E}_2 &= -e^{-(1+\lambda)s} \frac{U_2}{1 + y_2 e^{-(1+\lambda)s}}. \end{aligned}$$

¹Luo and Hou, consider instead the interior region $\{(r, x_3) \in r \leq 1, x_3 \in \mathbb{R}\}$ and assume periodicity in the x_3 direction. However, since the singularity is asymptotically local in nature, this difference should not play a role in the mechanism of the singularity.

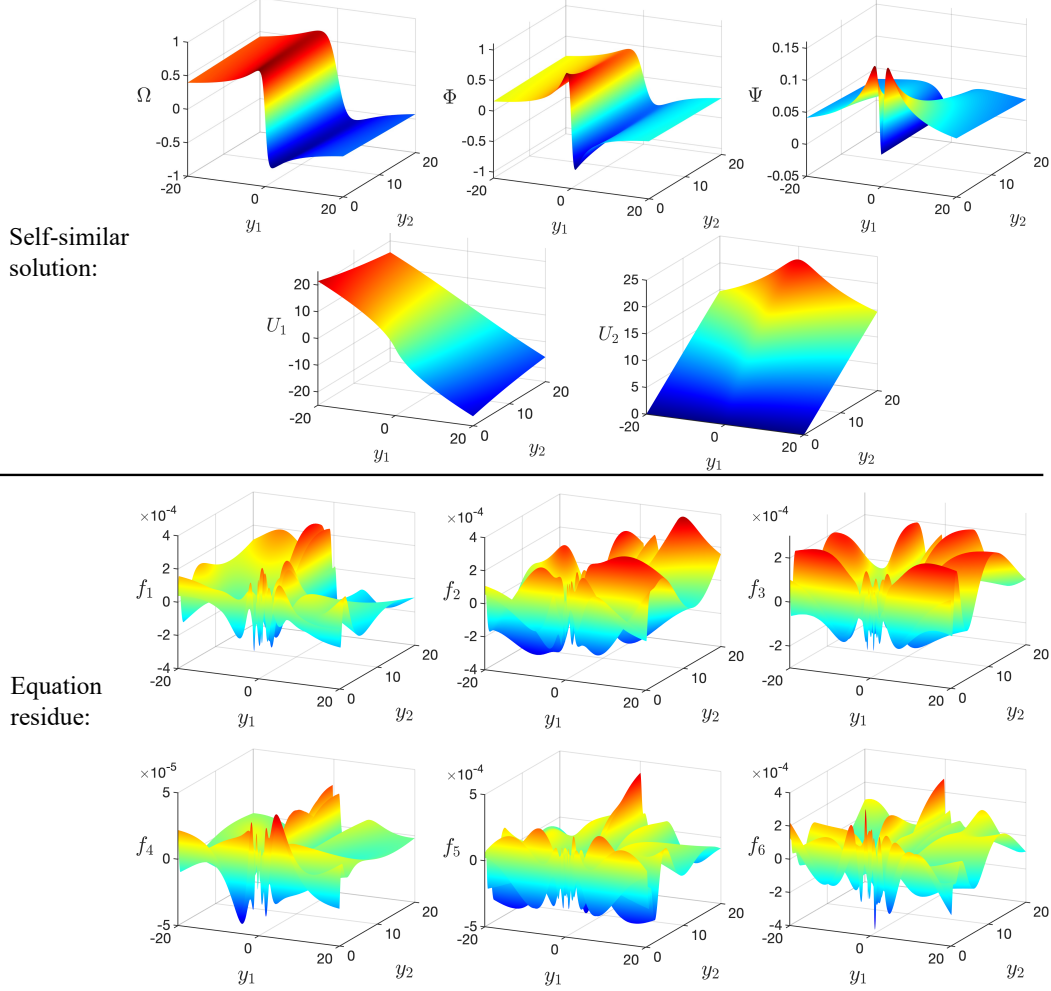


Figure 1: Smooth solution for the 2D Boussinesq equations (2.1) derived by the physics-informed neural network. f_1 to f_6 indicate the residue of the 6 equations defined in (3.3), which are around five orders of magnitude smaller than the output variables of the solution. The inferred value of λ for the smooth solution is $\lambda = 1.90$.

In the Luo-Hou scenario, we look for solutions which are asymptotically self-similar: i.e. in self-similar coordinates they converge to a stationary state as $s \rightarrow \infty$. For such solutions, for any fixed y , we have $\mathcal{E}_1, \mathcal{E}_2 = O(e^{-(1+\lambda)s})$ and thus the errors decay exponentially fast in self-similar coordinates assuming that $\lambda > -1$. In particular, the solutions converge pointwise to solutions of (2.1) as $s \rightarrow \infty$.

The above reasoning suggests that a self-similar blow-up solution for the Boussinesq can be used to construct an asymptotically self-similar solution for the Euler equations with cylindrical boundary. Indeed, such reasoning was carried out in [3] in order to construct non-smooth solutions for the Euler equations with cylindrical boundary.

2.2 Results

Figure 1 shows the plots of the approximate solutions to (2.1), along with their corresponding errors. The errors are approximately five orders of magnitude smaller than that of the solution found. The solutions are stable both with respect to the domain size and the random initialization. The solutions found appear to be in agreement with the asymptotics of the time dependent solutions found by Luo and Hou [22, 23]. Extrapolating from the paper [23], the work is suggestive of a self-similarity exponent of $\lambda \approx 2$ which

is in agreement with the exponent found by the PINN. As is the case for Luo and Hou, the trajectories corresponding to the self-similar velocity follow the geometry of a hyperbolic point at the origin.

3 Methods

To find the self-similar solution for the Bousinessq equation, we approximate U_1 , U_2 , Ω , Φ or Ψ in the Bousinessq equations (2.1) with fully-connected deep neural networks. Each network has two input variables y_1 and y_2 , which are the independent variables of the equations, and one output variable: U_1 , U_2 , Ω , Φ or Ψ . We add 6 hidden layers with 30 units in each layer for each network and use the hyperbolic tangent function \tanh as the activation function. To train the neural network to approach the exact solution, we define a cost function to quantify the difference between the neural network prediction and the target function, as well as an optimization algorithm that minimizes the cost function by updating the weights and biases in the neural networks throughout the training iterations.

For physics-informed neural networks, the cost function is defined by the mean square error and composed of two types of loss. The first type of loss is the *condition loss*, which evaluates the residue of the boundary conditions associated with the governing equations. Here, the residue of the condition is defined as the difference between the neural network approximated boundary condition and the true boundary condition. Mathematically, the condition loss can be written as

$$loss_c^{(j)} = \frac{1}{N_c^{(j)}} \sum_{i=1}^{N_c^{(j)}} g_{(j)}^2 \left[\mathbf{y}_i, \bar{q} \left(\mathbf{y}_i, \mathbf{w}^{(q)} \right) \right], \quad (3.1)$$

where $g_{(j)} \left(\mathbf{y}_i, \bar{q}(\mathbf{y}_i, \mathbf{w}^{(q)}) \right)$ indicates the residue of the j -th boundary condition at the i -th position $\mathbf{y}_i = (y_1, y_2)_i$ and $\bar{q} \left(\mathbf{y}_i, \mathbf{w}^{(q)} \right)$ is the neural network prediction. Here, $\mathbf{w}^{(q)}$ indicates the weights and biases of the neural network for any of the output variables q , i.e., U_1 , U_2 , Ω , Φ or Ψ . The parameter $N_c^{(j)}$ indicates the total number of points used for evaluating the j -th boundary condition. For example, the condition loss for the non-penetration boundary condition (2.2) reads,

$$loss_c^{(1)} = \frac{1}{N_c^{(1)}} \sum_{i=1}^{N_c^{(1)}} \left[\bar{U}_2 \left(\mathbf{y}_i, \mathbf{w}^{(U_2)} \right) - 0 \right]^2 \quad \text{with all } \mathbf{y}_i \text{ on the boundary } y_2 = 0.$$

The boundary conditions for the Bousinessq equation are listed in Section 2.

The second type of loss is known as the *equation loss*, which evaluates the residue of the governing equation averaged over a set of collocation points over the domain of calculation. Here, the residue of the equation $f_{(k)}$ is defined as the difference between the left and right-hand side of the equation calculated with the neural network predictions. The equation loss can be written as

$$loss_f^{(k)} = \frac{1}{N_f^{(k)}} \sum_{i=1}^{N_f^{(k)}} f_{(k)}^2 \left[\mathbf{y}_i, \bar{q} \left(\mathbf{y}_i, \mathbf{w}^{(q)} \right) \right], \quad (3.2)$$

where $f_{(k)} \left(\mathbf{y}_i, \bar{q}(\mathbf{y}_i, \mathbf{w}^{(q)}) \right)$ indicates the residue of the k -th equation evaluated at the i -th collocation point. The parameter $N_f^{(k)}$ denotes the total number of collocation points used for the k -th equation. For example, the equation loss of the first equation in (2.1) reads

$$loss_f^{(1)} = \frac{1}{N_f^{(1)}} \sum_{i=1}^{N_f^{(1)}} \left[\Omega \left(\mathbf{y}_i, \mathbf{w}^{(\Omega)} \right) + \left[(1 + \lambda) \mathbf{y}_i + \mathbf{U} \left(\mathbf{y}_i, \mathbf{w}^{(\mathbf{U})} \right) \right] \cdot \nabla \Omega \left(\mathbf{y}_i, \mathbf{w}^{(\Omega)} \right) - \Phi \left(\mathbf{y}_i, \mathbf{w}^{(\Phi)} \right) \right]^2$$

where $\mathbf{U} \left(\mathbf{y}_i, \mathbf{w}^{(\mathbf{U})} \right)$ indicates the neural network prediction of the velocity vector $\mathbf{U} = (U_1, U_2)$,

$$\mathbf{U} \left(\mathbf{y}_i, \mathbf{w}^{(\mathbf{U})} \right) = \left(U_1 \left(\mathbf{y}_i, \mathbf{w}^{(U_1)} \right), U_2 \left(\mathbf{y}_i, \mathbf{w}^{(U_2)} \right) \right).$$

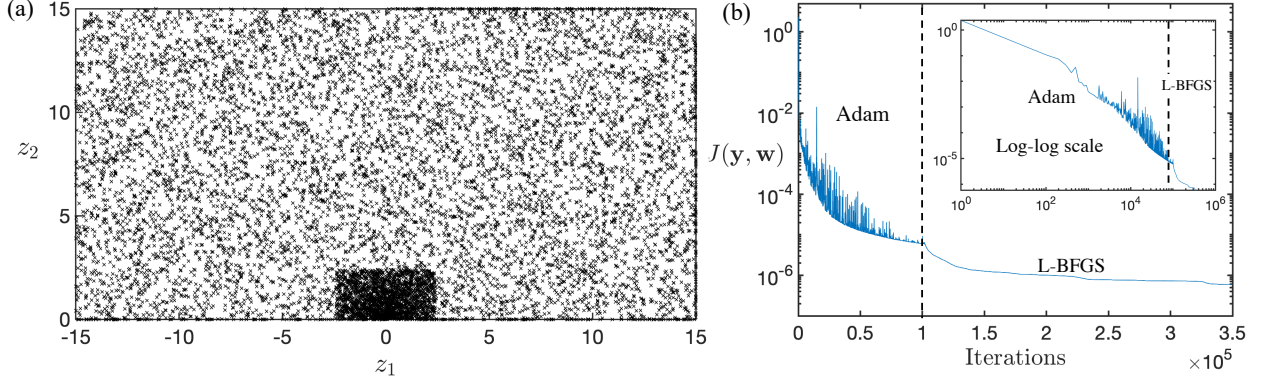


Figure 2: (a) Spatial distribution of the collocation points within the domain of calculation for the Bousinessq equations. Here (z_1, z_2) are the rescaled coordinates, with $y_1 = \sinh(z_1)$ and $y_2 = \sinh(z_2)$. There are 10,000 collocation points in total used in the PINN training for solving the Bousinessq equations. (b) Decrease of the total loss over the training iterations. The training uses both Adam and L-BFGS as the optimization methods. The inset shows the loss curve in a log-log scale.

All governing equations for the Bousinessq problem are listed in (2.1). Considering the definition of Ω and the fact that Φ and Ψ are the gradient components of Θ , we should evaluate the residue of 6 equations in total to guarantee the well-posedness of the problem for the PINN training, which are

$$\begin{aligned} f_1 &= \Omega + ((1 + \lambda)\mathbf{y} + \mathbf{U}) \cdot \nabla \Omega - \Phi, \\ f_2 &= (2 + \partial_{y_1} U_1) \Phi + ((1 + \lambda)\mathbf{y} + \mathbf{U}) \cdot \nabla \Phi + \partial_{y_1} U_2 \Psi, \\ f_3 &= (2 + \partial_{y_2} U_2) \Psi + ((1 + \lambda)\mathbf{y} + \mathbf{U}) \cdot \nabla \Psi + \partial_{y_2} U_1 \Phi, \\ f_4 &= \partial_{y_2} \Phi - \partial_{y_1} \Psi, \quad f_5 = \partial_{y_1} U_1 + \partial_{y_2} U_2, \quad \text{and} \quad f_6 = \Omega - (\partial_{y_1} U_2 - \partial_{y_2} U_1). \end{aligned} \quad (3.3)$$

The spatial distribution of the collocation points plays a critical role for the success of PINN training. To guide the neural network to approximate the correct self-similar solution for the Bousinessq equation (2.1), we train the neural network to prioritize the equation constraints around the origin. To reach this goal, we divide the domain into two regions, one close to the origin and one far, in each region the collocation points are uniformly distributed. We increase the number of collocation points surrounding the origin. Otherwise, there would be a high chance that the neural network prediction would be trapped in a local minimum during the training. In addition, to make sure the self-similar solution found by the PINNs is smooth over the domain, we also evaluate the gradient of the residue of all the Bousinessq equations (3.3) and add them into the equation loss, namely

$$loss_{\partial f}^{(k)} = \frac{1}{N_f^{(k)}} \sum_{i=1}^{N_f^{(k)}} \left| \nabla f_{(k)} \left(\mathbf{y}_i, \bar{q} \left(\mathbf{y}_i, \mathbf{w}^{(q)} \right) \right) \right|^2, \quad (3.4)$$

where $|\nabla f_{(k)}|$ indicates the magnitude of the gradient of the equation residue $f_{(k)}$, which reads

$$|\nabla f_{(k)}|^2 = (\partial_{y_1} f_{(k)})^2 + (\partial_{y_2} f_{(k)})^2.$$

Without loss of generality, we can use the same set of collocation points $N_f^{(k)}$ to evaluate the gradient of the residue for the k -th equation (3.4). Then, the sum of (3.1), (3.2) and (3.4) gives the final cost function $J(\mathbf{y}, \mathbf{w})$ for the PINN training,

$$J(\mathbf{y}, \mathbf{w}) = \frac{1}{n_b} \sum_{j=1}^{n_b} loss_c^{(j)} + \gamma \left(\frac{1}{n_e} \sum_{k=1}^{n_e} loss_f^{(k)} + \frac{1}{n_e} \sum_{k=1}^{n_e} loss_{\partial f}^{(k)} \right) \quad (3.5)$$

where n_b and n_e are the total number of boundary conditions and governing equations, respectively. In our case, this amounts to $n_b = 5$ and $n_e = 6$. The constant γ is a hyper-parameter of PINNs, known as the *equation weight* [29], which balances the contribution of the condition loss and equation loss in the final cost function $J(\mathbf{y}, \mathbf{w})$. For the Boussinesq equations, we choose $\gamma = 0.1$ for the optimal training performance.

The optimization methods for PINN training are based on gradient descent. Two commonly used approaches are *Adam* and *L-BFGS*. Adam [20], whose name is derived from the phrase *adaptive moment*, is a first-order gradient-based optimization algorithm based on adaptive estimates of lower-order moments. L-BFGS [21], standing for *Limited-memory Broyden-Fletcher-Goldfarb-Shanno* algorithm, is a quasi-Newton second-order gradient-based optimization method, which improves optimization using second derivatives. Despite the fact that no optimization method guarantees the convergence to a global minimum, our empirical experience, consistent with prior studies [25], shows that Adam performs better at avoiding local minima, while L-BFGS has a faster convergence rate throughout the training. Thus, we use Adam first for 100,000 iterations and then L-BFGS for 250,000 iterations to derive the self-similar solution for the Boussinesq equations. Figure 2(b) shows the convergence of the cost function $J(\mathbf{y}, \mathbf{w})$ throughout the training iterations.

The significant *advantages* of a PINN-based scheme compared to traditional numerical schemes to search for the self-similar solution are its universality and efficiency. For universality, the above PINN scheme can be generally applied to derive the self-similar solution for various equations without the requirement to know the specific structure of any particular equations. For efficiency, the smooth self-similar solution was in fact derived by PINN throughout one single training. There is no continuation scheme or time evolution required for the training, minimizing the computational cost of the training. We will give a robust validation of the universality and efficiency in the next section.

In this work, we use TensorFlow version 2.4.1 to perform the computation of the self-similar solution discovery via PINNs. The computations were conducted on one NVIDIA A100 40GB GPU provided by the Institute for Advanced Study. The computation time for obtaining the self-similar solution for the 2D Boussinesq equation as shown in Figure 1 is around 25 hours. For the 1D problems mentioned in the next section, the computation time is usually less than 20 minutes.

4 Validation of method for other models

In this section, we will validate our approach by comparing self-similar solutions obtained by the PINN to known results in the literature.

4.1 Non-smooth self-similar solutions for the Boussinesq equations

In [3], Chen and Hou constructed self-similar solutions for the Boussinesq equations lying in the space $C^{1,\alpha}$ for $\alpha > 0$ very small. The self-similar solutions are then used to prove blow-up for 3-D Euler in the presence of boundary. The work [3] is inspired by the earlier work of Elgindi [8] regarding self-similar solutions for the 3-D Euler in an unbounded domain. In upcoming work, Elgindi and Pasqualotto present a new blow-up scenario for non-smooth solutions to Boussinesq in the absence of boundary [13].

To describe Chen and Hou's result, we let fix $\alpha > 0$ small, set $\lambda = -1 + \frac{1}{\alpha}$ and define

$$R = (y_1^2 + y_2^2)^{\frac{\alpha}{2}} \quad \text{and} \quad \gamma = \arctan\left(\frac{y_2}{y_1}\right).$$

Chen and Hou then show that the self-similar Boussinesq equations (1.4) have an approximate solution given by²

$$\Omega = -\frac{\alpha}{c} (\cos(\gamma))^\alpha \frac{3R}{(1+R)^2}, \quad \Phi = -\frac{\alpha}{c} (\cos(\gamma))^\alpha \frac{6R}{(1+R)^3}, \quad \Psi \equiv 0 \quad (4.1)$$

²We remark that Chen and Hou [3] adopt the opposite sign convention for vorticity than that used in this paper.

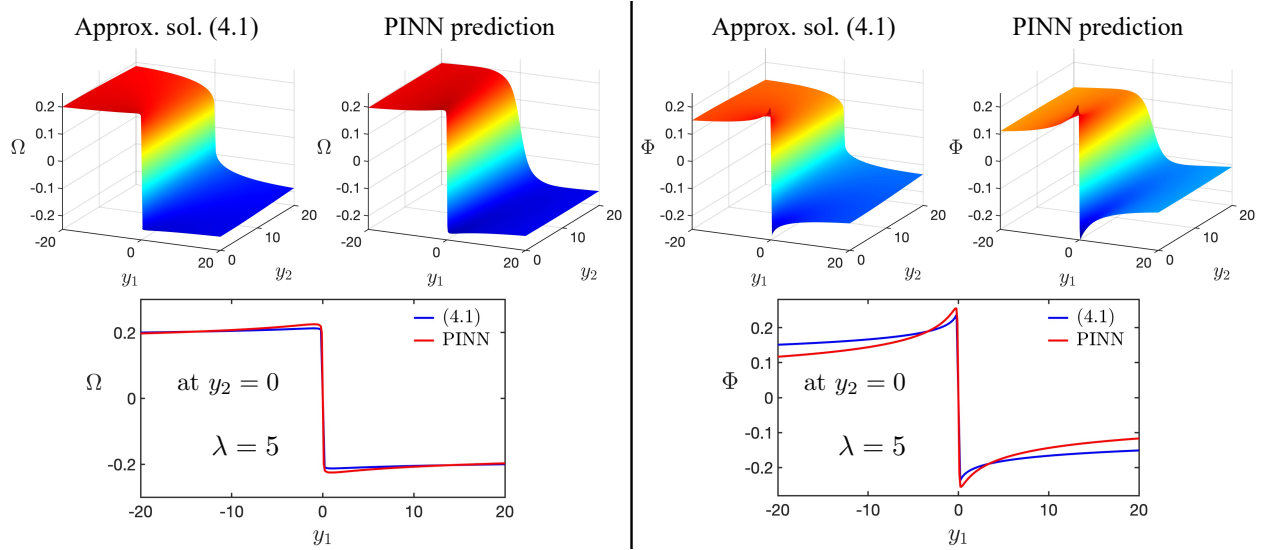


Figure 3: Non-smooth solutions of Ω and Φ for the 2D Bousinesq equations (2.1) derived by the physics-informed neural network for $\lambda = 5$, which shows an agreement with the approximate solution (4.1).

for $\gamma \in [0, \frac{\pi}{2}]$ (or equivalently $y_1 \geq 0$) and where

$$c = \frac{2}{\pi} \int_0^{\frac{\pi}{2}} (\cos(\theta))^\alpha \sin(2\theta) d\theta.$$

One then extends the approximate solution Ω and Φ to the region $y_1 \leq 0$ via an odd extension.

Figure 3 shows that for $\lambda = 5$, the solution found by the PINN agrees well with the approximation (4.1). In addition to providing an opportunity to validate the numerical method, the ability to find non-smooth solutions opens the possibility of using a continuation argument to search for smooth solutions. In the end, the PINN method is sufficiently robust that no such continuation argument is necessary; however, the possibility of such a continuation argument may be advantageous for other settings.

4.2 The Burgers' equation

One of the simplest PDEs which exhibits self-similar blow-up is the 1-D Burgers' equation:

$$u_t + uu_x = 0.$$

Assuming the self-similar ansatz

$$u = (1-t)^\lambda U\left(\frac{x}{(1-t)^{1+\lambda}}\right),$$

and defining y as in (1.3), we obtain the self-similar Burgers' equation

$$-\lambda U + ((1+\lambda)y + U)\partial_y U = 0. \quad (4.2)$$

The self-similar Burgers' equation may be implicitly solved, solutions are given by

$$y = -U - CU^{1+\frac{1}{\lambda}} \quad (4.3)$$

for some constant C . Removing a symmetry, we add the constraint

$$U(-2) = 1,$$

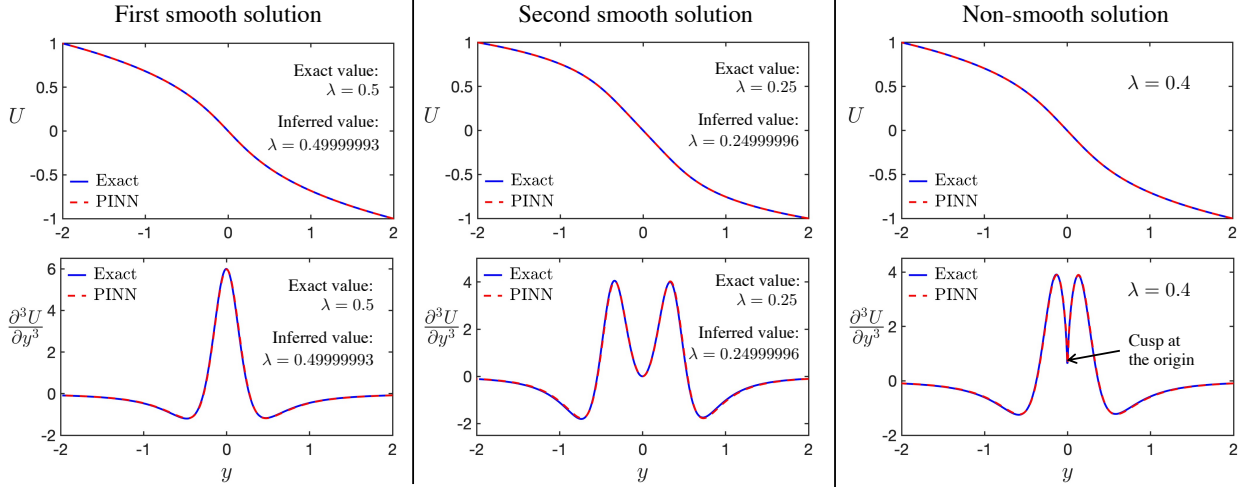


Figure 4: The first and second smooth solutions for the Burgers' equation using a physics-informed neural network. The error of the inferred λ for both smooth solutions is of order 10^{-7} . The right column shows that PINNs can successfully find the non-smooth solution for the Burgers' equation (i.e. $\lambda = 0.4$).

which fixes $C = 1$, independent of λ . It is classical [7], that in order to obtain a smooth self-similar solution, then λ must be chosen such that

$$\lambda = \frac{1}{2i+2} \quad \text{for } i = 0, 1, 2, \dots$$

Figure 4 demonstrates that the PINN is able to very accurately find the smooth solutions for the self-similar Burgers equation (4.2) along with their corresponding self-similar parameter λ . In order to find a specific smooth self-similar solution, we constrain the parameter λ to a window $\lambda \in [\frac{1}{2i+3}, \frac{1}{2i+1}]$. In addition to being able to find the smooth solutions to (4.2), the PINN can also accurately find the non-smooth solutions, which, as mentioned in Section 4.1, is a useful feature of the method. We also note that while the case $\lambda = \frac{1}{2}$ ($i = 0$) corresponds to stable, smooth self-similar profiles, the cases $i = 1, 2, \dots$ correspond to unstable self-similar profiles. A common numerical strategy to finding self-similar solutions is to introduce time dependence into the problem: while this is straightforward in the stable case, instabilities in the unstable case make finding unstable self-similar profiles comparatively more difficult if one is to employ such a strategy. The PINN method does not suffer this drawback and thus presents itself as great method for finding unstable smooth self-similar solutions. The self-similar Burgers' equation, being 1-D and local, is obviously a much simpler test for the PINN than the 2-D non-local self-similar Boussinesq equations; however, given that its solutions are given by a precise formula (4.3), the equation has proven to be an excellent sandbox to test and refine the PINN.

4.3 The generalized De Gregorio equation

Consider the generalized De Gregorio equation [26]

$$\omega_t + a u \omega_x = \omega u_x, \quad \text{where } u = \int_0^x (H\omega)(s) ds = \Lambda^{-1}\omega$$

and H is the Hilbert transform. The equation is a generalization of the De Gregorio equation ($a = 1$) [16] and has been proposed as a one-dimensional model for an equation for which there is nontrivial interaction of advection and vortex stretching (modeling behavior of the 3-D Euler equations).

The case $a = 0$, in the absence of advection, is known in the literature as the Constantin-Lax-Majda equation. In this particularly simple case, exact self-similar blow-up solutions can be constructed [5].

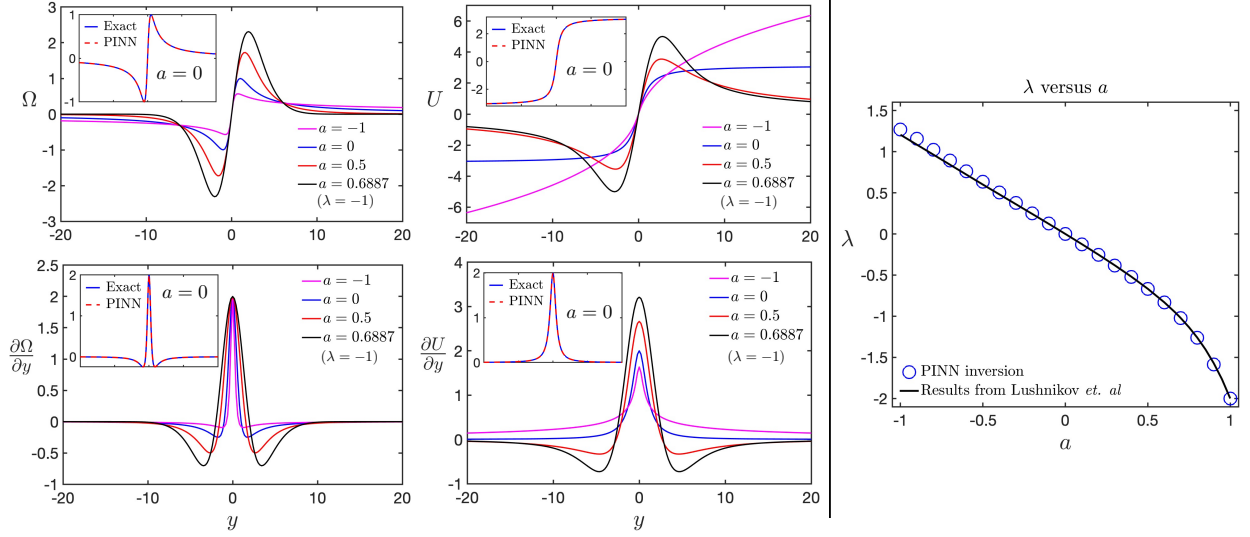


Figure 5: The left panel shows the smooth solution Ω and U of the generalized De Gregorio equation for different values of a . Besides inferring λ for a given value of a , PINN can also directly infer a for a given value of λ . The black line indicates the solution inferred by imposing $\lambda = -1$, which gives $a = 0.6887$, which shows a good agreement with the result from [24]. The inset shows the comparison of the PINN prediction with the exact solution for $a = 0$, which shows a perfect agreement. The right panel shows the curve of λ inferred via PINNs for different values of a within the range of $[-1, 1]$. The curve collapses well with the result from [24], indicating the accuracy of PINN inversion.

The case $a = -1$ was proposed as a model of the surface quasi-geostrophic (SQG) equation – it is known in the literature as the Córdoba-Córdoba-Fontelos model – and it also develops finite time singularities [6]. More generally, in the case $a < 0$, advection and vortex stretching do not compete but rather work in conjunction leading to finite time singularities [1]. The case $a > 0$ is more challenging, due to the competition of the two terms. By a clever expansion in a , smooth self-similar profiles were constructed in [10] for small, positive a , leading to finite time blowup. Via a computer-assisted proof, Chen, Hou, and Huang in [2] were able to show blow-up for the De Gregorio equation ($a = 1$).

The paper [24], represents the most thorough numerical study of equation (2.1) to date. In [24], self-similar solutions were found in the whole range $a \in [-1, 1]$ and beyond. We use their reported parameters as benchmarks for our results.

We assume the following self-similar ansatz

$$\omega = \frac{1}{1-t} \Omega \left(\frac{x}{(1-t)^{1+\lambda}} \right).$$

Then, if we define $U = \Lambda^{-1} \Omega$, make the change of coordinates (1.3), we obtain the self-similar equations

$$\Omega + ((1+\lambda)y + aU) \partial_y \Omega - \Omega \partial_y U = 0.$$

Note that the equation is invariant under the rescaling $\Omega(y) \mapsto \Omega(\mu y)$ (up to a change in λ). As such, we are free to fix

$$\partial_y \Omega(0) = 2. \quad (4.4)$$

We will assume that both Ω and U are odd.

Figure 5 demonstrates that the PINN can accurately reproduce the findings of [24], including the prediction that self-similar collapse forms for a below the critical value $a_c \approx 0.6887$. It should be noted that while the PINN can take advantage of a continuation argument in a in order to reduce computation

time, the PINN does not strictly require a continuation argument in order to find the self-similar solutions corresponding to $a = \pm 1$. As far as we know, this is the first such numerical method that can find such solutions without the aid of a continuation argument or a clever initialization of the iteration. This later fact is a further demonstration of the robustness of the method.

5 Conclusions and future work

For the first time, we are able to give a precise description of a smooth self-similar profile to the Boussinesq equations. Moreover, the profile represents an asymptotic self-similar profile for a Luo-Hou type blow-up scenario for the 3-D axi-symmetric Euler equations. The self-similar profile is found using a new numerical framework built on a physics-informed neural network. The framework is shown to be both robust and readily adaptable.

In future work, we aim to use our numerically computed approximate self-similar solution of (1.1) in a computer assisted proof of finite-time singularity formation from smooth finite energy initial data for both the Boussinesq equation and Euler equations with cylindrical boundary. Let $(U_0, \Theta_0, \lambda_0)$ be an approximate solution of (1.4) up to some small right-hand-side δ_0 . Using interval arithmetic, we can compute rigorous upper bounds on δ_0 . Given sufficient computational time, we hope to obtain an adequately precise solution $(U_0, \Theta_0, \lambda_0)$ of (1.4) with tight error bounds. In addition to such bounds on δ_0 , again by interval arithmetic, we will need to extract precise, rigorous spectral bounds on the linearization of (2.1) around the approximate solution $(U_0, \Theta_0, \lambda_0)$. The aim would then to use all these bounds to prove the existence of smooth finite energy initial data leading to a solution converging asymptotically to an exact solution of (1.4) in self-similar coordinates. Such a strategy was employed recently by Chen and Hou to prove finite-time blow-up for Boussinesq and Euler with cylindrical boundary in the case of non-smooth solutions [3] and we hope that a proof along these lines can be made to work in our case as well. See [4, 14] for additional examples where similar strategies have been employed in the context of fluid mechanics and [15] for a survey on computer-assisted proofs.

Our numerical strategy to find approximate self-similar solutions appears to be rather universal. It is our intention to employ the strategy in other settings in order to find new 2-D and 3-D self-similar solutions for fluid equations.

5.1 Acknowledgements

T.B. was supported by the NSF grant DMS-1900149 and a grant from the Institute for Advanced Study. This work was also supported by the Spanish State Research Agency, through the Severo Ochoa and María de Maeztu Program for Centers and Units of Excellence in R&D (CEX2020-001084-M). J.G.-S. received funding from the European Research Council (ERC) under the European Union’s Horizon 2020 research and innovation program through the grant agreement 852741. This material is based upon work supported by the National Science Foundation under Grant No. DMS-1929284 while J.G.-S. was in residence at the Institute for Computational and Experimental Research in Mathematics in Providence, RI, during the program “Hamiltonian Methods in Dispersive and Wave Evolution Equations”. Y.W. was supported by the Dean for Research Fund at Princeton University. T.B. and Y.W. were also supported by a Simons Foundation Mathematical and Physical Sciences Collaborative Grant. The simulations presented in this article were performed using the Princeton Research Computing resources at Princeton University and School of Natural Sciences Computing resources at the Institute for Advanced Study.

References

- [1] A. Castro and D. Córdoba, *Infinite energy solutions of the surface quasi-geostrophic equation*, Adv. Math. **225** (2010), no. 4, 1820–1829. MR2680191
- [2] J. Chen, T. Y. Hou, and D. Huang, *On the finite time blowup of the De Gregorio model for the 3d Euler equation*, arXiv preprint arXiv:1905.06387 (2019).
- [3] J. Chen and T. Y. Hou, *Finite Time Blowup of 2D Boussinesq and 3D Euler Equations with $C^{1,\alpha}$ Velocity and Boundary*, Communications in Mathematical Physics **383** (Apr. 2021), no. 3, 1559–1667.

- [4] J. Chen, T. Y. Hou, and D. Huang, *Asymptotically self-similar blowup of the Hou-Luo model for the 3D Euler equations*, arXiv e-prints (June 2021), arXiv:2106.05422, available at [2106.05422](https://arxiv.org/abs/2106.05422).
- [5] P. Constantin, P. D. Lax, and A. Majda, *A simple one-dimensional model for the three-dimensional vorticity equation*, Comm. Pure Appl. Math. **38** (1985), no. 6, 715–724. MR812343
- [6] A. Córdoba, D. Córdoba, and M. A. Fontelos, *Formation of singularities for a transport equation with nonlocal velocity*, Ann. of Math. (2) **162** (2005), no. 3, 1377–1389. MR2179734
- [7] J. Eggers and M. A. Fontelos, *The role of self-similarity in singularities of partial differential equations*, Nonlinearity **22** (2009), no. 1, R1–R44. MR2470260
- [8] T. Elgindi, *Finite-time singularity formation for $C^{1,\alpha}$ solutions to the incompressible Euler equations on \mathbb{R}^3* , Ann. of Math. (2) **194** (2021), no. 3, 647–727. MR4334974
- [9] T. M. Elgindi and I.-J. Jeong, *Finite-time singularity formation for strong solutions to the axis-symmetric 3d euler equations*, Annals of PDE **5** (Oct. 2019), no. 2.
- [10] T. M. Elgindi and I.-J. Jeong, *On the effects of advection and vortex stretching*, Archive for Rational Mechanics and Analysis **235** (Oct. 2019), no. 3, 1763–1817.
- [11] T. M. Elgindi and I.-J. Jeong, *Finite-Time Singularity Formation for Strong Solutions to the Boussinesq System*, Annals of PDE **6** (May 2020), no. 1.
- [12] T. M. Elgindi, T.-E. Ghoul, and N. Masmoudi, *On the Stability of Self-similar Blow-up for $C^{1,\alpha}$ Solutions to the Incompressible Euler equations on \mathbb{R}^3* (2019), available at [1910.14071](https://arxiv.org/abs/1910.14071).
- [13] T. M. Elgindi and F. Pasqualotto (2022). Personal communication.
- [14] A. Enciso, J. Gómez-Serrano, and B. Vergara, *Convexity of Whitham’s highest cusped wave*, arXiv e-prints (Oct. 2018), arXiv:1810.10935, available at [1810.10935](https://arxiv.org/abs/1810.10935).
- [15] J. Gómez-Serrano, *Computer-assisted proofs in PDE: a survey*, SeMA J. **76** (2019), no. 3, 459–484. MR3990999
- [16] S. D. Gregorio, *A partial differential equation arising in a 1d model for the 3d vorticity equation*, Mathematical Methods in the Applied Sciences **19** (Oct. 1996), no. 15, 1233–1255.
- [17] J. Guillod and V. Šverák, *Numerical investigations of non-uniqueness for the Navier-Stokes initial value problem in borderline spaces*, arXiv:1704.00560 (2017).
- [18] K. Hornik, M. Stinchcombe, and H. White, *Multilayer feedforward networks are universal approximators*, Neural networks **2** (1989), no. 5, 359–366.
- [19] G. E. Karniadakis, I. G. Kevrekidis, L. Lu, P. Perdikaris, S. Wang, and L. Yang, *Physics-informed machine learning*, Nature Reviews Physics **3** (May 2021), no. 6, 422–440.
- [20] D. P. Kingma and J. Ba, *Adam: A method for stochastic optimization*, arXiv preprint arXiv:1412.6980 (2014).
- [21] D. C. Liu and J. Nocedal, *On the limited memory BFGS method for large scale optimization*, Mathematical programming **45** (1989), no. 1, 503–528.
- [22] G. Luo and T. Y. Hou, *Potentially singular solutions of the 3D axisymmetric Euler equations*, Proceedings of the National Academy of Sciences **111** (2014), no. 36, 12968–12973, available at <https://www.pnas.org/content/111/36/12968.full.pdf>.
- [23] G. Luo and T. Y. Hou, *Toward the finite-time blowup of the 3D axisymmetric Euler equations: a numerical investigation*, Multiscale Model. Simul. **12** (2014), no. 4, 1722–1776. MR3278833
- [24] P. M. Lushnikov, D. A. Silantiev, and M. Siegel, *Collapse Versus Blow-Up and Global Existence in the Generalized Constantin–Lax–Majda Equation*, Journal of Nonlinear Science **31** (Aug. 2021), no. 5.
- [25] S. Markidis, *Physics-informed deep-learning for scientific computing*, arXiv preprint arXiv:2103.09655 (2021).
- [26] H. Okamoto, T. Sakajo, and M. Wunsch, *On a generalization of the Constantin–Lax–Majda equation*, Nonlinearity **21** (2008), no. 10, 2447–2461. MR2439488
- [27] M. Raissi, P. Perdikaris, and G. E. Karniadakis, *Physics-informed neural networks: A deep learning framework for solving forward and inverse problems involving nonlinear partial differential equations*, Journal of Computational Physics **378** (Feb. 2019), 686–707.
- [28] M. Raissi, A. Yazdani, and G. E. Karniadakis, *Hidden fluid mechanics: Learning velocity and pressure fields from flow visualizations*, Science **367** (Jan. 2020), no. 6481, 1026–1030.

- [29] R. van der Meer, C. W Oosterlee, and A. Borovykh, *Optimally weighted loss functions for solving pdes with neural networks*, Journal of Computational and Applied Mathematics (2021), 113887.
- [30] V. I. Yudovich, *Eleven great problems of mathematical hydrodynamics*, 2003, pp. 711–737, 746. Dedicated to Vladimir I. Arnold on the occasion of his 65th birthday. MR2025281